

ADIABATIC SHEAR BANDS IN FUNCTIONALLY GRADED MATERIALS

R. C. Batra and B. M. Love

*Department of Engineering Science and Mechanics
Virginia Polytechnic Institute
and State University
Blacksburg, Virginia, USA*

The initiation and propagation of adiabatic shear bands (ASBs) in functionally graded materials (FGMs) deformed at high strain rates in plane-strain tension have been studied. An ASB is a narrow region, usually a few micrometers wide, of intense plastic deformation that forms after softening of the material due to its being heated up and the evolution of damage in the form of porosity has overcome its hardening due to strain and strain-rate effects. An FGM is usually composed of two or more constituents with material properties varying continuously through it; the one studied here is made of tungsten particles interspread in a NiFe matrix. Each constituent and the composite are modeled as heat-conducting, microporous, strain and strain-rate hardening, and thermally softening materials with material parameters of the composite derived from those of its constituents by the rule of mixtures. They obey the Johnson–Cook thermoviscoplastic relation, the Gurson-type flow potential, the associated flow rule, and a hyperbolic heat equation. The degradation of thermophysical parameters with the evolution of damage is accounted for with porosity representing the damage. With origin at the centroid of a square cross section, the volume fraction of each phase is assumed to vary radially until a boundary point on the square cross section is reached and then to stay constant. It is found that an ASB, aligned along the direction of the maximum shear stress, forms sooner in an FGM than in either of the two constituent materials with its location, orientation, pattern, and speed depending on the compositional profile.

Keywords coupled large transient thermomechanical deformations, finite element solution, shear strain localization, thermoviscoplasticity

Received 2 February 2004; accepted 20 April 2004.

This work was partially supported by Office of Naval Research grants N00014-98-1-0300 and N0014-03-MP-2-0131, Army Research Office grant DAAD19-01-1-0657, and the Air Force Office of Scientific Research – Multi University Research Initiative subcontract from Georgia Institute of Technology to Virginia Polytechnic Institute and State University. Opinions expressed in the paper are those of the authors and not of funding agencies.

Address correspondence to R. C. Batra, Department of Engineering Science and Mechanics, M/C 0219, Virginia Polytechnic Institute and State University, Blacksburg, VA 24061, USA. E-mail: rbatra@vt.edu

Tresca [1] observed hot lines now called adiabatic shear bands (ASBs) during the hot forging of a platinum bar; they were subsequently also observed by Massey [2]. Even though heat conduction plays a significant role in determining the width of an ASB and possibly spacing between adjacent bands, the adjective adiabatic is used to signify that they form rapidly in a body deformed at a high strain rate and that there may not be enough time for the heat to be conducted away. Their study is important because they precede ductile fracture. The research activity in ASBs increased subsequent to Zener and Hollomon observing them [3] during the punching of a hole in a steel plate. They also postulated that a material point becomes unstable when thermal softening equals the combined hardening due to strain and strain-rate effects. Several earlier investigations (e.g., see [4]) have used this criterion to determine the average strain at the time of initiation of an ASB and to rank materials according to their susceptibility to shear banding; under identical loadings a material in which an ASB forms sooner is more susceptible to shear banding. Bai [5] studied simple shearing deformations of a homogeneous thermoviscoplastic body, neglected elastic deformations, perturbed the homogeneous solution of the governing equations, and hypothesized that an ASB forms when infinitesimal perturbations grow. Batra and Chen [6] have shown that this approach gives the same result as that proposed by Zener and Hollomon [3]. Experimental observations of Marchand and Duffy [7] on the torsion of thin-walled tubes have revealed that an ASB forms much later than when the shear stress peaks and is accompanied by a rapid drop in the torque required to deform the tube. Numerical solutions of simple shearing, plane-strain, and axisymmetric problems [8] and torsional deformations of a thin-walled tube [9] have confirmed that the load-carrying capacity of a member drops significantly upon the formation of an ASB. Much of the literature on ASBs can be found in two books [10, 11], a review paper [12], and special issues of journals [13–17].

One of the earlier papers on functionally graded materials (FGMs) is that of Hasselman and Youngblood [18], who showed that the thermal stress resistance of a structural ceramic can be enhanced by properly grading the thermal conductivity. Most works on FGMs have analyzed thermoelastic deformations of platelike structures (e.g., see [18–29]), and those on ASBs have focused on analyzing their initiation and propagation in a homogeneous body. We note that Batra and Zhu [30–32] studied ASBs in a laminated composite body. Here we analyze the problem for an FGM composed of two constituents with the compositional profile and, hence, material properties varying continuously in a cross section. A goal is to find compositions that either enhance or delay the initiation of an ASB. Whereas in a monolithic body, deformations become inhomogeneous due to the interaction of waves reflected from boundaries with the incident waves, in an FGM the additional source of nonuniform deformations is the spatial variation of material properties. In an FGM composed of particulates in a matrix, waves are also reflected from numerous interfaces between the two phases. The interaction among waves and the sudden change in properties of two constituents give inhomogeneous deformations of the body. However, here a functionally graded (FG) body with continuous variation of material properties is considered. Thus, the wave speed varies continuously from point to point and waves are reflected only from the boundaries. The deformations are inherently inhomogeneous.

It is found that the compositional profile noticeably affects the time of initiation, the direction of propagation, and the material point from where an ASB forms relative to that in a homogeneous body composed of each constituent. Furthermore, an ASB forms sooner in an FGM than in either one of the two constituents. Thus, materials of desired susceptibility to adiabatic shear banding can be designed.

FORMULATION OF THE PROBLEM

Governing Equations

We use rectangular Cartesian coordinates and the referential description of motion to describe transient coupled thermomechanical deformations of an elastothermoviscoplastic FG body deformed at a high strain rate in plane-strain tension. Deformations of each constituent and the composite body are governed by the following equations expressing, respectively, the balance of mass, the balance of linear momentum, the balance of moment of momentum, and the balance of internal energy.

$$\rho(1 - f)J = \rho_0(1 - f_0) \tag{1}$$

$$\rho_0(1 - f_0)\dot{v}_i = T_{i\alpha,\alpha} \quad i, j = 1, 2, \quad \alpha = 1, 2 \tag{2}$$

$$T_{i\alpha}F_{j\alpha} = T_{j\alpha}F_{i\alpha} \tag{3}$$

$$\rho_0(1 - f_0)\dot{e} = -Q_{\alpha,\alpha} + T_{i\alpha}\dot{F}_{i\alpha} \tag{4}$$

where ρ is the present mass density, f is the porosity (i.e., the volume fraction of voids), $J = \det \mathbf{F}$, $F_{i\alpha} = x_{i,\alpha} = \partial x_i / \partial X_\alpha$ is the deformation gradient, \mathbf{x} is the present position at time t of a material particle located at the place \mathbf{X} in the reference configuration, \mathbf{T} is the first Piola–Kirchhoff stress tensor, e is the specific internal energy, \mathbf{Q} is the present heat flux measured per unit reference area, \mathbf{v} is the velocity of a material particle, a superimposed dot indicates the material time derivative, and a repeated index implies summation over the range of the index. Greek indices refer to coordinates in the reference configuration, and Latin indices refer to coordinates in the present configuration.

We assume that the strain-rate tensor \mathbf{D} , defined by $D_{ij} = (v_{i,j} + v_{j,i})/2$, $v_{i,j} = \partial v_i / \partial x_j$, has the additive decomposition into an elastic part \mathbf{D}^e and a plastic part \mathbf{D}^p , namely,

$$\mathbf{D} = \mathbf{D}^e + \mathbf{D}^p \tag{5}$$

Equations (1)–(5) are supplemented with the following constitutive relations:

$$\dot{\sigma}_{ij} + \sigma_{ik}W_{kj} - \sigma_{jk}W_{ik} = \frac{E(1 - f)}{1 + \nu} D_{ij}^e + \frac{E(1 - f)\nu}{(1 + \nu)(1 - 2\nu)} (D_{kk}^e - \hat{\alpha}\dot{\theta})\delta_{ij} \tag{6}$$

$$\dot{e} = c\tau\dot{\theta} + c\dot{\theta} + \frac{1}{\rho(1 - f)} \sigma_{ij}D_{ij}^e \tag{7}$$

$$T_{ix} = J\sigma_{ij}(F^{-1})_{aj} \tag{8}$$

$$q_i = -\kappa\left(1 - \frac{3}{2}f\right)\theta_{,i} \quad Q_\alpha = Jq_i(F^{-1})_{\alpha i} \tag{9}$$

$$\begin{aligned} \phi &\equiv \frac{\sigma_e^2}{\sigma_y^2} - 1 + 2f^*\beta_1 \cosh\left(\frac{\beta_2\bar{p}}{2\sigma_y}\right) - \beta_1^2(f^*)^2 = 0 \\ \sigma_e^2 &= \frac{3}{2}\sigma'_{ij}\sigma'_{ij} \quad i, j = 1, 2, 3 \end{aligned} \tag{10}$$

$$D_{ij}^p = \dot{\lambda} \frac{\partial \phi}{\partial \sigma_{ij}} = \dot{\lambda} \left[\frac{3\sigma'_{ij}}{\sigma_y^2} - \frac{f^*\beta_1\beta_2}{\sigma_y} \sinh\left(\frac{\beta_2\bar{p}}{2\sigma_y}\right) \delta_{ij} \right] \quad \sigma'_{ij} = \sigma_{ij} + p\delta_{ij} \tag{11}$$

$$p = -(\sigma_{11} + \sigma_{22} + \sigma_{33})/3 \quad \bar{p} = pH(-p - 0) \tag{12}$$

$$\dot{\lambda} = \begin{cases} \frac{(1-f)\sigma_y\dot{\epsilon}_e^p}{\sigma_{ij}(\partial\phi/\partial\sigma_{ij})} & \text{if } \phi = 0 \text{ and } \dot{\phi} \geq 0 \\ 0 & \text{when either } \phi < 0 \text{ or } \phi = 0 \text{ and } \dot{\phi} < 0 \end{cases} \tag{13}$$

$$\dot{f} = (1-f)D_{ii}^p + \frac{f_2\dot{\epsilon}_e^p}{s_2\sqrt{2\pi}} e^{-\frac{1}{2}\left(\frac{f_u - f_n}{s_2}\right)^2} H(-p - 0) \tag{14}$$

$$f^* = \begin{cases} f & f \leq f_c \\ f_c + \frac{f_u - f_c}{f_f - f_c}(f - f_c) & f > f_c \end{cases} \tag{15}$$

$$\sigma_y = (A + B(\epsilon_e^p)^n) \left(1 + C \ln\left(\frac{\dot{\epsilon}_e^p}{\dot{\epsilon}_0^p}\right)\right) \left(1 - \left(\frac{\theta - \theta_\tau}{\theta_m - \theta_\tau}\right)^m\right) \tag{16}$$

where the left-hand side of Eq. (6) equals the Jaumann derivative of the Cauchy stress tensor σ ; $W_{ij} = (v_{i,j} - v_{j,i})/2$ is the spin tensor, E is Young’s modulus, ν is Poisson’s ratio, $\hat{\alpha}$ is the coefficient of thermal expansion, θ is the temperature rise, δ_{ij} is the Kronecker delta, c is the specific heat, τ is the thermal relaxation time, κ is the thermal conductivity of the solid material, and θ is the present temperature of a material particle. Batra and Jaber [33] found that the Jaumann and the Green–Naghdi stress rates in Eq. (6) give virtually identical results for the times of initiation of an ASB and of brittle failure at points near the surface of a notch tip in a dynamically loaded prenotched plate. This is because elastic strain rates

appearing in Eq. (6) are small compared to the plastic strain rates at points within an ASB. $\phi = 0$ describes the yield surface proposed by Gurson [34] for a porous material, p is the hydrostatic pressure, and f^* is the modified value of the porosity given by Eq. (15). Gurson's yield surface is based on quasi-static analysis with the matrix material modeled as rigid perfectly plastic and obeying the von Mises yield criterion. Wang and Jiang [35] have considered inertia effects. Wang [36] has analyzed transient deformations of a single spherical void in a solid spherical shell made of a power-law heat-conducting viscoplastic material. For a microporous material, Wang [36] derived an approximate expression for the macrostress potential through an upper bound approach. Constants β_1 and β_2 , introduced by Tvergaard [37], provide a better fit of results computed from a finite element analysis of the formation of ASBs in a plate having an array of large cylindrical voids with test observations, and λ is the factor of proportionality defined by Eqs. (13); $\lambda > 0$ only when the material point is deforming plastically; σ_y is the current yield stress of the material whose dependence on the effective plastic strain ϵ_e^p , the effective plastic strain rate $\dot{\epsilon}_e^p$, and the temperature θ is described by Johnson–Cook [38] relation (16) in which A , B , C , $\dot{\epsilon}_e^p$, and m are material parameters, θ_r is the room temperature, and θ_m is the melting temperature of the material. Parameters B and n characterize the strain hardening of the material, C and $\dot{\epsilon}_0^p$ characterize the strain-rate hardening, and the last factor on the right-hand side of Eq. (16) is thermal softening. Equation (14) gives the evolution of porosity; the first term on its right-hand side is derived by assuming that the matrix is incompressible and the elastic dilatation is negligible compared to the plastic dilatation, and the second term is the strain-based nucleation of voids introduced by Chu and Needleman [39]. f_2 , s_2 , and ϵ_n are material parameters; the rate of nucleation of voids is highest when $\dot{\epsilon}_e^p$ equals ϵ_n and decays exponentially with the difference between $\dot{\epsilon}_e^p$ and ϵ_n . H is the Heaviside step function. Thus, the second term contributes to the evolution of porosity at a point only when the hydrostatic pressure there is tensile. To account for the coalescence of neighboring voids, Tvergaard and Needleman [40] enhanced the porosity, as given by Eq. (15), after it reaches its critical value f_c . In Eq. (15), f_f is the porosity at ductile fracture, and $f_u = 1/\beta_1$ is the porosity when the yield surface has shrunk to a point. Equations (10) and (16) imply that the radius of the von Mises yield surface increases due to strain and strain-rate hardening of the material but decreases due to the softening induced by the temperature rise and the increase in porosity. The degradation of material properties due to the damage, taken here to be synonymous with the porosity, is indicated by Eqs. (6)–(10). The affine variation with the porosity of Young's modulus, the bulk modulus, the stress–temperature coefficient, and the heat capacity implies that the rule of mixture has been employed to find their effective values; the expression for the thermal conductivity in Eq. (9) is due to Budiansky [41]. The interaction, if any, among neighboring voids has been tacitly ignored. Jiang and Batra [42], among others, have considered this interaction. The shrinkage of the yield surface due to an increase in porosity described by Eq. (10) can be seen by plotting the yield surface for two different values of f while keeping other variables fixed. Perzyna [43] has given a different equation for the evolution of porosity.

For an FG body, all thermophysical parameters may vary with \mathbf{X} .

Substitution from Eqs. (5), (7), and (9) into Eq. (4) gives the following hyperbolic heat equation:

$$\rho_0(1-f_0)c(\tau\ddot{\theta} + \dot{\theta}) = \left(\kappa \left(1 - \frac{3}{2}f \right) \theta_{,z} \right)_{,z} + J\sigma_{ij}D_{ij}^p \quad (17)$$

The term $J\sigma_{ij}D_{ij}^p$ equals the heating due to plastic working per unit volume in the reference configuration; thus, the Taylor–Quinney parameter has been taken as 1. Except for a delay in the time of initiation of an ASB, other results remain unaffected by a lower value of the Taylor–Quinney factor. The form of hyperbolic heat equation (17) is due to Cattaneo [44] and Vernotte [45]. The thermal relaxation time τ represents the time required to establish a steady state of heat conduction in an element suddenly exposed to heat flux. According to Chester [46] τ equals $3\kappa/\rho cV_0^2$, where V_0 is the speed of an elastic wave. Thus, for a typical steel, $\tau = 1 \times 10^{-12}$ s, and $\tau \simeq 25 \times 10^{-12}$ s for copper. Batra and Lear [47] and Batra and Chen [48] found that the finiteness of the thermal wave speed affects the time of initiation of an ASB in a typical steel and the spacing between adjacent shear bands only when $\tau \geq 10^{-6}$ s. Batra [49] considered higher order spatial and temporal gradients of temperature and derived a heat equation that admits finite speeds of thermal waves. However, in such a material either a thermal wave propagates with a finite speed or the linearized problem has a unique solution. Ideally, one likes to have both.

We note that Batra and Kim [50], Batra and Jaber [33] and Batra and Chen [6] have analyzed different aspects of shear banding with four different thermovisco-plastic relations, namely, the Johnson–Cook [38], the Litonski–Batra (e.g., see [51]), the Bodner–Partom [52], and a power law. These relations were calibrated to give nearly the same effective stress versus the effective strain curve during homogeneous deformations of the body. However, during inhomogeneous deformations, each one of the relations gave qualitatively similar but quantitatively different results. The decision to use the Johnson–Cook relation here is based on the availability of values of thermomechanical parameters for different materials.

Initial and Boundary Conditions

For a prismatic body having a uniform square cross section (i.e., volume fractions of constituents are independent of the axial coordinate) and initial and boundary conditions independent of the axial coordinate, it is reasonable to assume that a plane-strain state of deformation prevails in the body. Furthermore, thermomechanical deformations are assumed to be symmetric about the two centroidal axes. Thus the compositional profile has been tacitly assumed to be symmetric about the two centroidal axes. Deformations of only a quarter of the cross section in the first quadrant, shown shaded in Figure 1, are analyzed with boundary conditions (18)_{10–15} arising from the symmetry of deformations imposed at points on the centroidal axes. The other vertical surface $X_1 = H$ is taken to be traction free and thermally insulated; see Eqs. (18)_{8,9}. Normal velocity, null tangential tractions, and zero heat flux are prescribed on the top horizontal surface $X_2 = H$; these are given by Eqs. (18)_{15–17}. The prescribed normal velocity, given by Eq. (18)₁₇, increases

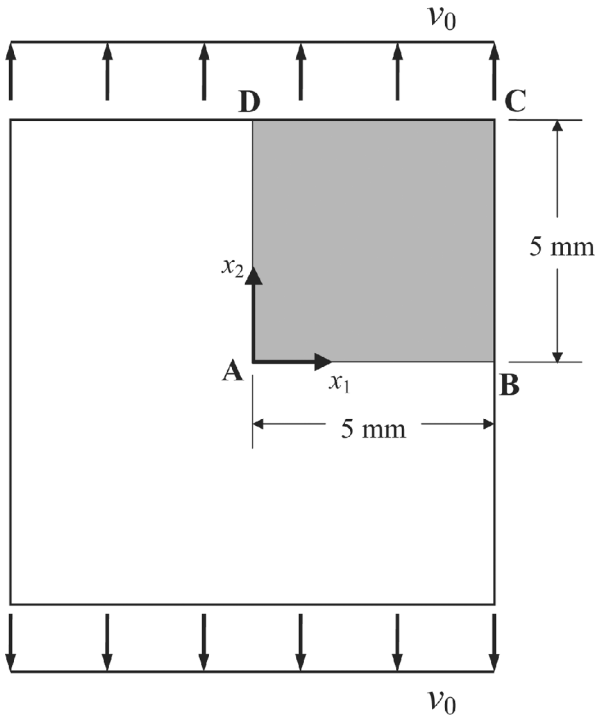


Figure 1. Schematic sketch of the problem studied.

linearly with time to its steady-state value v_0 in $1 \mu s$ and is then held fixed. The body is initially at rest, at a uniform temperature, and has zero initial porosity (cf. Eqs. (18)₁₋₇). Thus,

$$\begin{aligned}
 \mathbf{x}(\mathbf{X}, 0) &= \mathbf{X} & \mathbf{v}(\mathbf{X}, 0) &= \mathbf{0} & \theta(\mathbf{X}, 0) &= \theta_0 & \dot{\theta}(\mathbf{X}, 0) &= 0 & \rho(\mathbf{X}, 0) &= \rho_0 \\
 \varepsilon_e^p(\mathbf{X}, 0) &= 0 & f(\mathbf{X}, 0) &= f_0(\mathbf{X}) & (X_1, X_2) &\in [0, H] \times [0, H] \\
 T_{21} &= T_{11} = 0 & Q_1 &= 0 & \text{on } X_1 &= H \\
 T_{21} &= 0 & v_1 &= 0 & Q_1 &= 0 & \text{on } X_1 &= 0 \\
 T_{12} &= 0 & v_2 &= 0 & Q_2 &= 0 & \text{on } X_2 &= 0 \\
 T_{12} &= 0 & Q_2 &= 0 & v_2 &= \begin{cases} v_0 t, & 0 \leq t \leq 1 \mu s \\ v_0, & t \geq 1 \mu s \end{cases} & \text{on } X_2 &= H
 \end{aligned} \tag{18}$$

Nondimensionalization of Variables

Let $\rho_R, \dot{\varepsilon}_R, H, \sigma_0,$ and θ_R be the reference mass density, the reference strain rate, the reference length, the reference stress, and the reference temperature used to

nondimensionalize quantities. Then in terms of nondimensional variables indicated by the same symbols as before, Eqs. (2) and (17) become

$$\alpha_I(1-f_0)\dot{v}_i = T_{i\alpha,\alpha} \quad i = 1, 2 \quad \alpha = 1, 2 \quad (19)$$

$$\rho_0(1-f_0)(\tau\ddot{\theta} + \dot{\theta}) = -\alpha_t \left(\left(1 - \frac{3}{2}f\right)\theta_x \right)_{,\alpha} + J\sigma_{ij}D_{ij}^p \quad i, j = 1, 2, 3 \quad (20)$$

where

$$\alpha_I = \frac{\rho_R \dot{\epsilon}_R^2 H^2}{\sigma_0} \quad \alpha_t = \frac{\kappa}{\rho_R c H^2 \dot{\epsilon}_R} \quad \theta_R = \frac{\sigma_0}{\rho_R c H^2 \dot{\epsilon}_R} \quad (21)$$

and α_I and α_t are nondimensional measures of inertia and heat conduction effects, respectively. For a given material, inertia effects are directly proportional to the square of the reference strain rate and the square of the reference length, and heat conduction effects are inversely proportional to the reference strain rate and the square of the reference length. A possible choice for $2H$ is the length of a side of the square cross section, and that for $\dot{\epsilon}_R$ is v_0/H .

Homogenization of Material Properties

We first analyzed transient deformations of a representative volume element (RVE) to evaluate effective properties of the composite as a function of the volume fraction of constituents. Values of material parameters characterizing elastic deformations so determined were found to match well with those given by the Mori–Tanaka [53] scheme. However, values of material parameters characterizing the plastic deformation could not be satisfactorily determined from deformations of the RVE. We thus use the rule of mixtures to evaluate values of all material parameters from those of the constituents and their volume fractions. According to this rule, the value P of a material parameter for a mixture composed of two constituents with volume fractions V_1^f and V_2^f and values P_1 and P_2 of the material parameter is given by

$$P = V_1^f P_1 + V_2^f P_2 = (1 - V_2^f)P_1 + V_2^f P_2 \quad (22)$$

which gives exact values of the mass density and the heat capacity, is simple to use, and often gives an upper bound for values of other material parameters for the composite. It ignores interactions among adjacent particulates, their shapes and sizes, and their distribution in the matrix.

Suquet [54] has given a closed-form expression for the yield stress of an isotropic homogenized body made of isotropic elastic perfectly plastic constituents. The estimate of the yield stress involves effective shear modulus of the composite. For a tungsten/NiFe FG body, the difference in the effective yield stress computed from Suquet's expression and that obtained by the rule of mixtures is less than 10%.

Semi-discrete Formulation of the Problem

Equations (6), (8), and (3) imply that the balance of moment of momentum (3) is identically satisfied. The present mass density can be computed from Eq. (1) if the

deformation gradient and the current value of the porosity are known. Thus, the dependent variables to be solved for are \mathbf{x} , f , and θ and the independent variables are \mathbf{X} and t . Equations (19) and (20) are second-order coupled non-linear hyperbolic partial differential equations for \mathbf{x} and θ . These cannot be written explicitly in terms of \mathbf{x} and θ since \mathbf{T} is given by Eq. (8) and $\boldsymbol{\sigma}$ by Eq. (6), which involve \mathbf{D}^p and θ . To solve the problem numerically by the finite element method (FEM), we first derive its weak or variational formulation.

Let $\mathbf{w}(\mathbf{X})$ be a smooth function that is an analog of virtual velocity. We take the inner product of Eq. (19) with \mathbf{w} , integrate the resulting equation over the region Ω occupied by the body in the reference configuration, and use the divergence theorem and the natural boundary conditions in Eqs. (18) to arrive at

$$\int_{\Omega} \alpha_I (1 - f_0) \dot{v}_i w_i \, d\Omega = - \int_{\Omega} w_{i,\alpha} T_{i\alpha} \, d\Omega \tag{23}$$

Let $\psi_1, \psi_2, \dots, \psi_n$ be finite element (FE) basis functions defined on Ω . We write

$$v_i = \sum_{A=1}^{\text{nodes}} \psi_A(\mathbf{X}) \tilde{v}_{Ai}(t) \quad w_i = \sum_{A=1}^{\text{nodes}} \psi_A(\mathbf{X}) c_{Ai} \quad i = 1, 2 \tag{24}$$

where $\tilde{\mathbf{v}}$ is the vector of velocities of nodes, and c 's are constants. Substituting from Eq. (24) into Eq. (23) and exploiting the fact that the resulting equation must hold for all choices of \mathbf{c} , we get

$$\begin{aligned} \mathbf{M}\dot{\tilde{\mathbf{v}}} &= -\mathbf{F}^{\text{int}} \\ M_{AB} &= \int_{\Omega} \alpha_I (1 - f_0) \psi_A \psi_B \, d\Omega \quad F_{Ai}^{\text{int}} = \int_{\Omega} \psi_{A,\alpha} T_{i\alpha} \, d\Omega \end{aligned} \tag{25}$$

To derive a weak form of Eq. (25) we first introduce an auxiliary variable

$$\xi = \dot{\theta} \tag{26}$$

and follow the same procedure as that used to derive Eq. (25)₁, with the following result:

$$\begin{aligned} \dot{\theta} &= \tilde{\xi} \\ \tau \mathbf{H} \dot{\tilde{\xi}} + \mathbf{H} \tilde{\xi} &= \mathbf{F}^{\theta} + \tilde{\mathbf{Q}} \end{aligned} \tag{27}$$

where

$$\begin{aligned} H_{AB} &= \int_{\Omega} \rho_0 (1 - f_0) \psi_A \psi_B \, d\Omega \\ F_A^{\theta} &= \int_{\Omega} \alpha_I \left(1 - \frac{3}{2} f \right) \theta_{,\alpha} \psi_{A,\alpha} \, d\Omega \\ Q_A &= \int_{\Omega} \psi_A J \, \text{tr}(\boldsymbol{\sigma} \mathbf{D}^p) \, d\Omega \end{aligned} \tag{28}$$

Note that the natural boundary condition of zero heat flux has been embedded in Eq. (27)₂.

We solve Eq. (16) for $\dot{\epsilon}_e^p$ in terms of σ_y , ϵ_e^p , and θ and derive its weak form in the same way as before except that the divergence theorem is not used. Recall that $\dot{\epsilon}_e^p > 0$ only when a material point is deforming plastically as signified by the satisfaction of Eq. (10)₁; otherwise, $\dot{\epsilon}_e^p = 0$. Weak forms of Eqs. (6), (14), and

$$\dot{\mathbf{x}} = \mathbf{v}(\mathbf{X}, t) \quad (29)$$

are also derived. We thus get coupled nonlinear ordinary differential equations

$$\dot{\mathbf{d}} = \mathbf{F} \quad (30)$$

where \mathbf{d} is the vector of unknowns and \mathbf{F} is the force vector that depends on time t and $\mathbf{d}(t)$. The twelve unknowns at a node are $\{x_1, x_2, v_1, v_2, \sigma_{11}, \sigma_{22}, \sigma_{12}, \sigma_{33}, f, \theta, \zeta, \epsilon_e^p\}$.

ASB Initiation Criterion

Batra and Rattazzi [55] studied the initiation and propagation of an ASB in a prenotched thick-walled steel tube and found that the choice of the ASB initiation criterion will affect the predicted initiation time. They used four different criteria: (i) the effective plastic strain at a point equals 0.5, (ii) the effective plastic strain at a point equals 1.0, (iii) the effective stress at a point has dropped to 90% of its peak value at that point, and (iv) the effective stress at a point has dropped to 80% of its maximum value at that point; in each case the material point must be deforming plastically. Criteria (iii) and (iv) reflect Marchand and Duffy's [7] observation that the torque required to twist thin-walled tubes drops precipitously upon the initiation of an ASB. Batra and Kim [56] scrutinized ASBs in 12 materials deformed in simple shear and proposed criterion (iv), which we use in the present work.

COMPUTATION AND DISCUSSION OF RESULTS

Compositional Profile

Results have been computed for tungsten (W) particles interspread in NiFe matrix with the volume fraction of NiFe, $v_{f, NiFe}$, given by one of the following two expressions:

$$v_{f, NiFe} = \begin{cases} \text{Type I} \\ c_f \frac{r}{H} & r \leq H \\ c_f & r \geq H \end{cases} \quad v_{f, NiFe} = \begin{cases} \text{Type II} \\ c_f \left(1 - \frac{r}{H}\right) & r \leq H \\ 0 & r \geq H \end{cases} \quad (31)$$

where r is the radial distance from the specimen centroid, and $2H = 10$ mm is the length of a side of the square cross section. In both type I and type II FGMs, material properties in the region $r > H$ are constants. In type I FGMs, the volume fraction of NiFe varies from zero at the specimen centroid to c_f at $r = H$, and, in type II FGMs, it varies from c_f at the specimen centroid to zero at $r = H$. The material is homogeneous in the region $r \geq H$.

The primary reason for studying compositional profile (31) is that it does not influence the direction of propagation of an ASB originating from the centroid of the cross section. For the same overall volume fraction of the constituents, the ASB initiation time may depend on the distribution of the two constituents. If an ASB does not initiate from the centroid, then distribution (31) of NiFe may affect the direction of propagation of the ASB.

Validation of the Computer Code

A computer code based on the semidiscrete formulation described earlier, employing four-node quadrilateral elements, has been developed. Integrals in Eqs. (25) and (28) are first written as the sum of integrals over each element; the latter are evaluated by using the 2×2 Gauss quadrature rule. The variation of material properties with \mathbf{X} is accounted for by using their values at a quadrature point when evaluating integrals in Eqs. (25) and (28) numerically. Sharp spatial gradients in material parameters can be captured either by using a very fine FE mesh or by employing a higher order integration rule. Batra [57] employed a similar technique to analyze finite deformations of an FG cylindrical pressure vessel made of an Mooney–Rivlin material. Consistent mass and heat capacity matrices are employed. Recall that natural boundary conditions are embedded in Eqs. (30). Equations (30) are modified to enforce prescribed velocity components at nodes on the bounding surfaces and are then integrated by using the subroutine (Livermore Solver for Ordinary Differential Equations LSODE) with parameter MF in LSODE set equal to 10 and parameters ATOL = RTOL = 10^{-7} . ATOL and RTOL control the absolute and the relative tolerances in the computed solution. MF = 10 implies that the subroutine uses the Adams–Moulton method for integrating ordinary differential equations. LSODE adaptively adjusts the size of the time step and the order of the method to compute the solution within the prescribed accuracy. The subroutine can be downloaded from the Internet.

The computer code was validated by comparing computed results with the published ones and also by using the method of so-called manufactured solutions in which body forces and sources of internal energy density can be found for any assumed deformation and temperature fields. These and initial and boundary conditions corresponding to the assumed solution are input into the code. The computed solution should match the presumed analytical solution of the problem (e.g., see [58], Eq. (20), and a few lines following it). Furthermore, the solution for an ASB problem in a homogeneous body essentially coincided with Batra and Lear's [47] solution obtained with an FE mesh of triangular elements.

To ascertain the effect of the FE mesh on the ASB initiation time, we analyzed deformations of type I FGM with $c_f = 0.3$ in Eq. (31) with three different uniform FE meshes. As is clear from the results summarized in Table 1, the ASB initiation time decreased by 2.1% in going from a 40×40 to 120×120 uniform FE mesh, and the CPU time increased by a factor of 21. Results presented in subsequent sections are with a 40×40 uniform FE mesh of four-node isoparametric quadrilateral elements.

Table 1 Effect of FE mesh on the ASB initiation time for type I FGM with $c_f = 0.3$

Uniform FE mesh	ASB initiation time (μs)	CPU time (s)	% change in ASB initiation time
40×40	65.9	1,133	—
80×80	64.8	6,908	1.67
120×120	64.5	29,242	2.12

ASBs in Five Homogeneous Materials

For homogeneous materials, Batra and Lear [47] assumed the presence of 2% initial porosity at the specimen centroid, which decayed exponentially to zero with the distance from the centroid. Because of the maximum initial porosity, the centroid acts as a nucleation site for an ASB. However, for a composite, deformations naturally become inhomogeneous because of the spatial variation of material properties and it determines where and when an ASB initiates. For reference and to delineate the effect of the initial porosity distribution, we have listed in Table 2 values of material parameters and in Table 3 the nondimensional ASB initiation times (or, equivalently, the average axial strain) for five materials deformed at an average axial strain rate of 5,000/s. For $H = 5$ mm, the axial speed v_0 was increased from 0 to 25 m/s in $1 \mu\text{s}$ and then kept constant. It is clear that an ASB initiates considerably sooner in initially porous materials than in those with zero initial porosity. Nondimensional inertia factor α_I is higher for NiFe, Armco iron, and Oxygen free high conductivity (OFHC) copper than for 4340 steel and tungsten even though the mass density of tungsten is almost twice that of steel. Heat conduction effects are higher in OFHC copper than in any of the other four materials studied; it is reflected in the delayed initiation of an ASB in copper. The rather high nondimensional thermal conductivities of NiFe and Armco iron also delay the onset of ASBs in them. The nondimensional thermal conductivities of tungsten and NiFe are nearly the same but α_I for tungsten is about one-fifth of that for NiFe. A clear correlation among the ASB initiation time, α_I , and α_t has not been established yet. We note that the ASB initiation time also depends on the nominal axial strain rate.

Figure 2 exhibits the time history of the applied axial load for the five materials; the axial strain plotted along the abscissa equals the time multiplied by the nominal axial strain rate. In each case the initiation of an ASB is accompanied by a rapid drop in the axial load; the rate of drop of the axial load is higher for tungsten than that for any of the other four materials. In each case, the ASB initiated from the centroid of the cross section. The porosities at the instant of the ASB initiation were 0.041, 0.087, 0.081, 0.126, and 0.155, respectively, in W, NiFe, 4340 steel, Fe, and Cu; the temperature rise is listed in Table 3. An approximate value of the temperature rise is given by $((A + 0.5B(\epsilon_e^p)^n)\epsilon_e^p)/(\rho c)$ since the effect of heat conduction until an ASB initiates is small. It also provides a check on the accuracy of computed results. For W, the temperature rise computed from this relation at the time of initiation of an ASB is 368 K.

Table 2 Values of thermomechanical parameters for the five materials studied

Material	A (MPa)	B (MPa)	C	m	n	θ_m (K)	α ($10^{-5}/K$)	κ (W/mK)	c (J/kgK)	ρ (kg/m ³)	ν	E (GPa)	α_f (10^{-3})	α_f (10^{-6})
4340 steel	792.19	509.51	0.014	1.03	0.26	1793	12.3	38	477	7840	0.27	210	6.19	81.3
Armco iron	175.12	379.99	0.060	0.55	0.32	1811	12.1	73	452	7890	0.29	196	28.16	163.8
OFHC copper	89.63	261.64	0.031	1.09	0.31	1356	17.0	386	383	8960	0.33	120	62.48	899.9
Tungsten	1505.79	176.50	0.016	1.00	0.12	1723	4.3	75	134	17000	0.20	406	7.06	263.4
Nickel iron	150.0	546.0	0.0838	1.0	0.208	1225	15.0	100	382	9200	0.29	255	38.33	227.6

* Values for an average axial strain of 5,000/s, $H = 5$ mm, and $\sigma_0 = A$.

Table 3 Axial strain at ASB initiation in five homogeneous materials deformed in plane-strain tension at a nominal strain rate of 5,000/s

Material	Axial strain at ASB initiation		Temperature rise (K) at ASB initiation (present work)
	with initial porosity	without initial porosity (present work)	
Tungsten	0.137	0.386	391
4340 steel	0.315	0.615	315
Nickel iron	—	0.944	354
OFHC copper	0.391	1.045	157
Armco iron	0.433	1.095	253

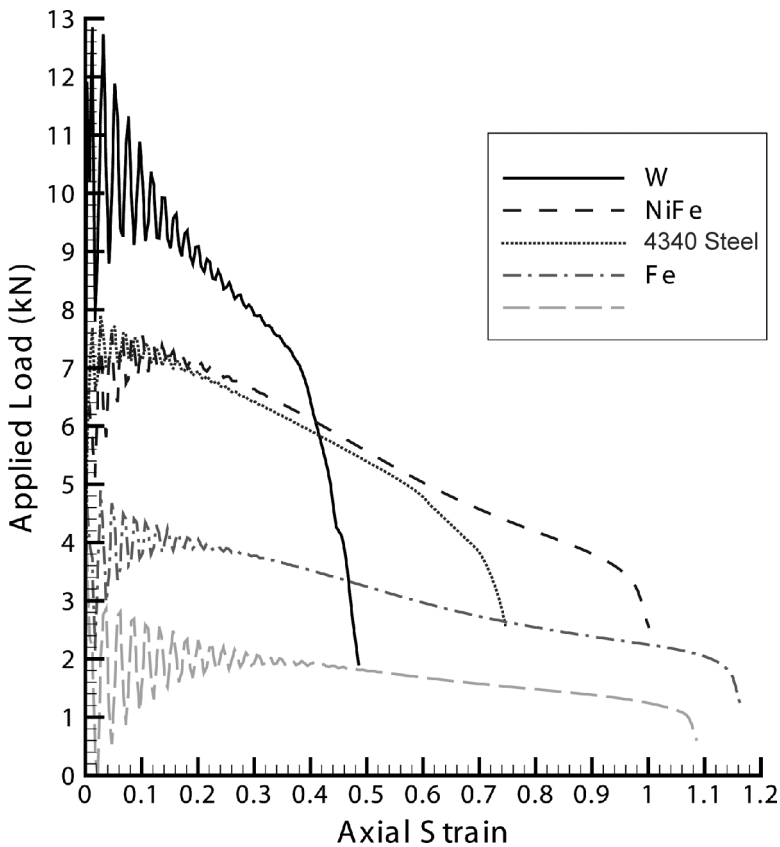


Figure 2. Axial load vs. average axial strain for five homogeneous materials deformed in plane-strain tension.

ASBs in FGMS

Numerical experiments on type I and type II FGMS yielded interesting results which are summarized in Table 4. In type I FGMS, there is 100% W at $r=0$, and the volume fraction of NiFe equals 0 at $r=0$ and increases linearly with r reaching its maximum value at $r=H$; the maximum volume fraction of NiFe at $r=H$ varies from 0.1 to 0.5. In each case, an ASB initiated at the specimen centroid and propagated along a line inclined at approximately 45° to the horizontal axis in the present configuration. The axial strain at the instant of ASB initiation decreased when the maximum volume fraction of NiFe at $r=H$ was increased from 0.1 to 0.4, and then increased a little when c_f in Eq. (31) was increased from 0.4 to 0.5. However, in each case, the average axial strain at the instant of the ASB initiation is less than that for the pure W. It leads one to conjecture that the addition to W of a material less susceptible to shear banding than W increases tungsten's susceptibility to shear banding. To test this conjecture, numerical experiments were performed on type I FGMS with NiFe replaced by 4340 steel, Cu, and Fe. The spatial distribution of the volume fraction of W was kept the same. Whereas in each FGM the ASB initiated sooner than that in pure W, the decrease in the time of initiation of an ASB cannot be simply related to the times of initiation of ASBs in the constituents.

Contours of the effective plastic strain in type I FGMS are depicted in Figure 3. The effective plastic strain within the ASB exceeds 1 with a peak value of 1.5 at some points. The necking of the region below the ASB is evident in these plots.

Results for numerical experiments on other type I FGMS containing different matrix material are also summarized in Table 4.

For type II FGMS with the maximum volume fraction of NiFe at the centroid, an ASB initiated from a point on the top surface and propagated inward along the two directions of the maximum shear stress. These seem to get reflected from the surfaces $X_1=0, H$. As shown in Figure 4, there are several narrow regions of large plastic deformation. For the first three FGMS, the point where an ASB initiates on the top surface varies with the compositional profile. For the other two FGMS, an ASB initiates from a point within the cross section. Fully developed ASBs exhibited in Figure 4 reveal that the eventual distribution of regions of intense plastic deformation is independent of c_f . The time of initiation of an ASB decreases monotonically with an increase in the maximum volume fraction, c_f , of NiFe. However, the rate of decrease of the time of initiation decreases rapidly as c_f is increased from 0.1 to 0.5. In contrast to FGMS of type I, necking occurs in the upper part rather than in the lower portion of the cross section.

Figure 5 depicts contours of the effective plastic strain in type I FGMS with the matrix material either 4340 steel, OFHC copper or Fe. A comparison of these plots with those in Figure 3 reveals that an ASB initiates from a point on the top surface in these cases as opposed to from the centroid when the matrix is NiFe. As listed in Table 4, the point of initiation of the ASB varies with the matrix material. Of the FGMS studied, the type I with NiFe matrix delays most the onset of an ASB and that with Fe matrix the least. Composites comprised of W in the region $r < 5$ mm and NiFe elsewhere or vice versa were also analyzed. ASBs initiated in these two composites at much lower values of the average axial strain than in all of the FGMS

Table 4 Axial strain and the point of initiation of ASBs in FGMs

Specimen type and constituents	Max. v_f of matrix	Axial strain at ASB initiation	Location of ASB initiation (ref. config.)	
			X	Y
W/NiFe type I	0.1	0.371	0.000	0.000
	0.2	0.339	0.000	0.000
	0.3	0.327	0.000	0.000
	0.4	0.325	0.000	0.000
	0.5	0.331	0.000	0.000
W/NiFe type II	0.1	0.340	1.125	5.000
	0.2	0.314	1.250	5.000
	0.3	0.304	1.375	5.000
	0.4	0.298	4.750	2.875
	0.5	0.292	4.875	2.875
W/4340 steel type I	0.3	0.364	1.125	5.000
W/Cu type I	0.3	0.218	0.625	5.000
W/Fe type I	0.3	0.268	1.000	5.000
W, $r < 5$	—	0.194	2.875	4.000
NiFe, $r > 5$	—	0.154	4.875	1.500

and in the two homogeneous bodies. Recall that material properties are discontinuous across the surface $r=H$. It suggests that the presence of a material singular surface enhances the initiation of an ASB. The gradients of displacements and temperature must be discontinuous across $r=H$ for surface tractions and the normal component of the heat flux to be continuous.

The significant difference between the initiation times of ASBs in the two composites with W in the region $r < 5$ mm and NiFe in $r > 5$ mm or vice versa cannot be explained on the basis of the arrival time of the elastic loading wave since $\sqrt{E/\rho}$ is nearly the same for W and NiFe. However, their acoustic impedances $\sqrt{E\rho}$ are quite different. Batra and Kwon [59] scrutinized the initiation and development of ASBs in simple shearing deformations of a bimetallic body with the lower half made of one thermoviscoplastic material and the upper half of a different thermoviscoplastic material. For both materials having the same value of the shear modulus and the mass density, they found that the ASB developed in the body with the higher value of the thermal softening coefficient even though the initial nonuniform temperature was symmetric about the centerline and maximum at the center. The differences in thermal conductivities shifted the ASB a little. No shift in the center of the ASB away from the centerline occurred even when the shear modulus of one material was twice that of the other material. The data included in the last two rows of Table 4 indicate that an ASB initiated at the point (2.875, 4.0), or $r = 4.93$ mm when W occupied the region $r < 5$ mm, and at the point (4.875, 1.50), or $r = 5.10$ mm for W in the region $r > 5$ mm. The coordinates of points are in the reference configuration. These results agree with those of Batra and Kwon [59]. Zhou et al. [60] analyzed numerically and experimentally plane-strain deformations of a particulate composite composed of W particles in NiFe matrix and modeled each constituent as a

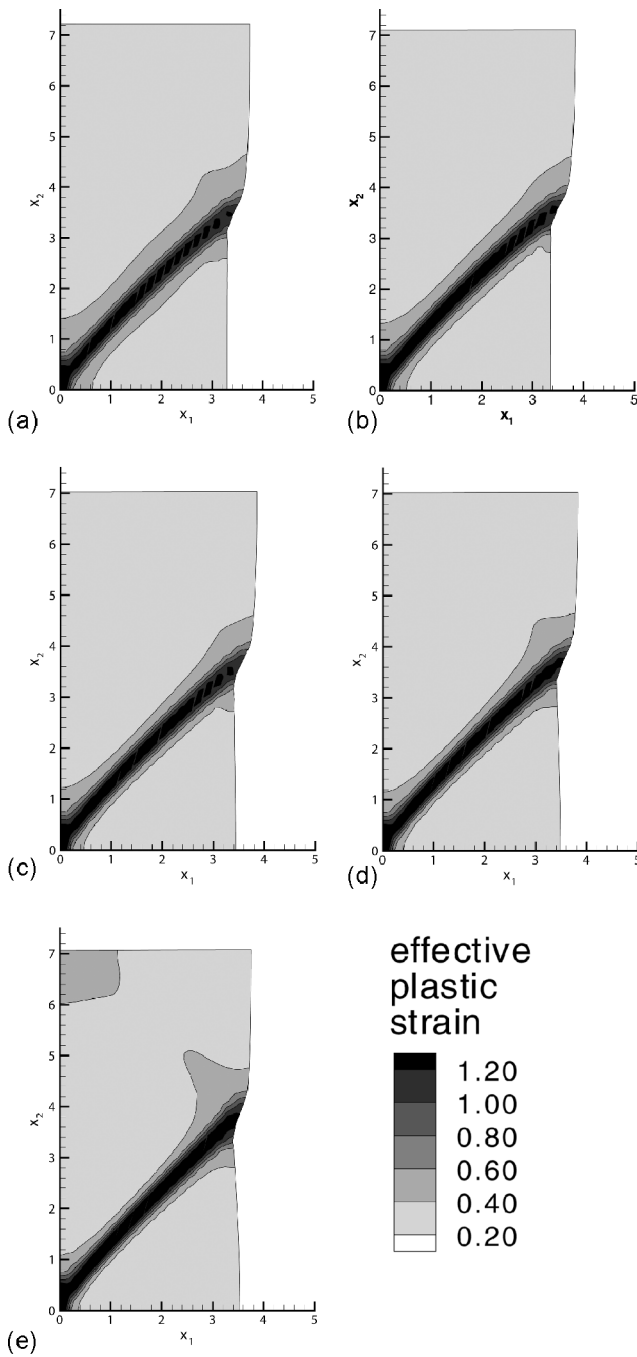


Figure 3. Contours of the effective plastic strain in type I FGMs with the maximum volume fraction of NiFe at $r=H$ equal to (a) 0.1, (b) 0.2, (c) 0.3, (d) 0.4, and (e) 0.5.

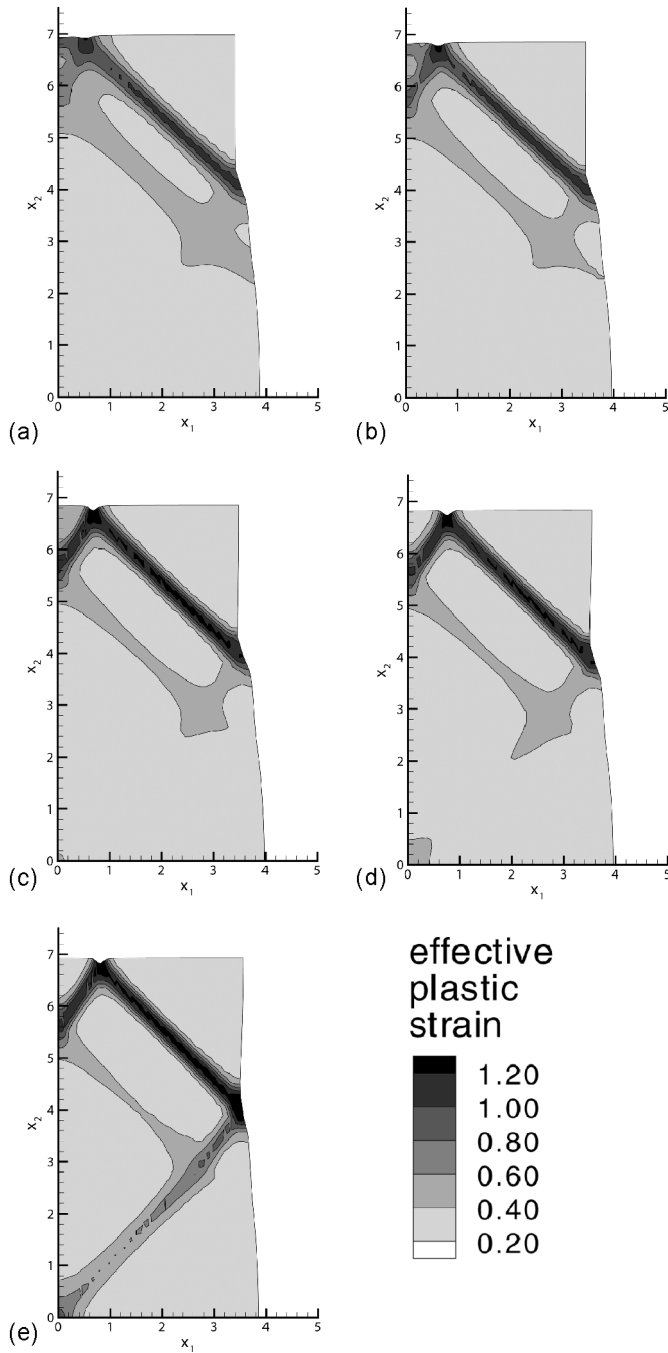


Figure 4. Contours of the effective plastic strain in type II FGMs with the maximum volume fraction of NiFe at $r=0$ equal to (a) 0.1, (b) 0.2, (c) 0.3, (d) 0.4, and (e) 0.5.

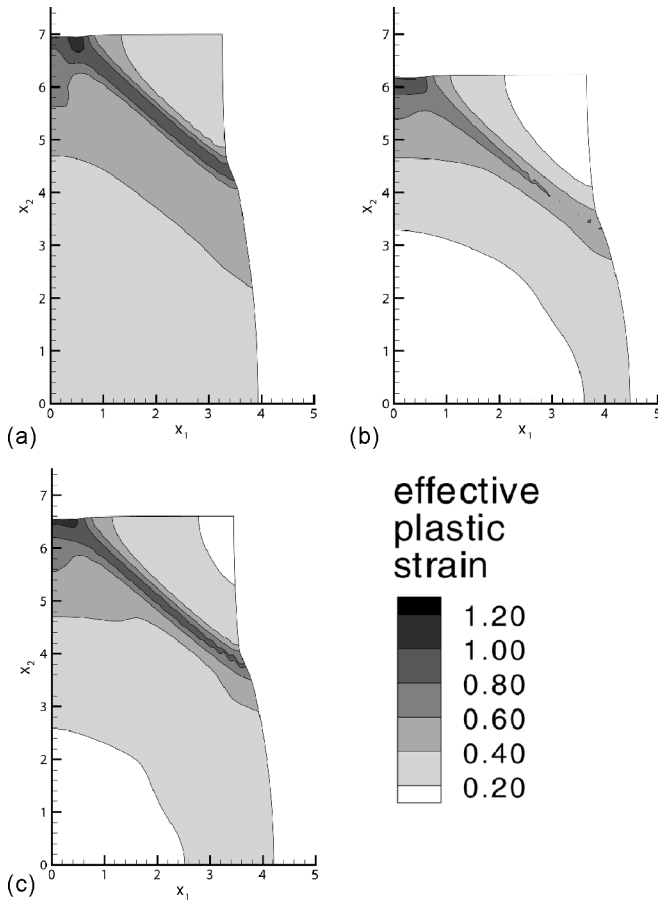


Figure 5. Contours of the effective plastic strain in type I FGMs with the maximum volume fraction of W at $r=H$ equal to 0.7 and (a) 4340 steel, (b) Cu, and (c) Fe as the other constituent.

thermoviscoplastic material. Thus, there were several surfaces of discontinuity present in the body. They also found that an ASB initiated sooner in the composite than in either one of the two constituents. They neither homogenized material properties nor investigated the effect of the spatial variation of the volume fraction of the two constituents, nor did they consider the evolution of porosity.

An ASB initiates from the point at the center of the shaded area in Figure 6a. The shaded zones in Figures 6b–6d depict the shear banded regions. Since the length of this region increases in both directions around the point shown in Figure 6a, one can conclude that the shear band propagates outward in both directions.

For each problem studied, the time step was seen to drop drastically once an ASB had initiated at a point in the body. The numerical values of the ASB initiation time may depend on the FE mesh employed. However, differences in results from a much finer mesh than the one used here are likely to be less than 5% because the ASB initiation time obtained with 6400 uniform elements differed from that with

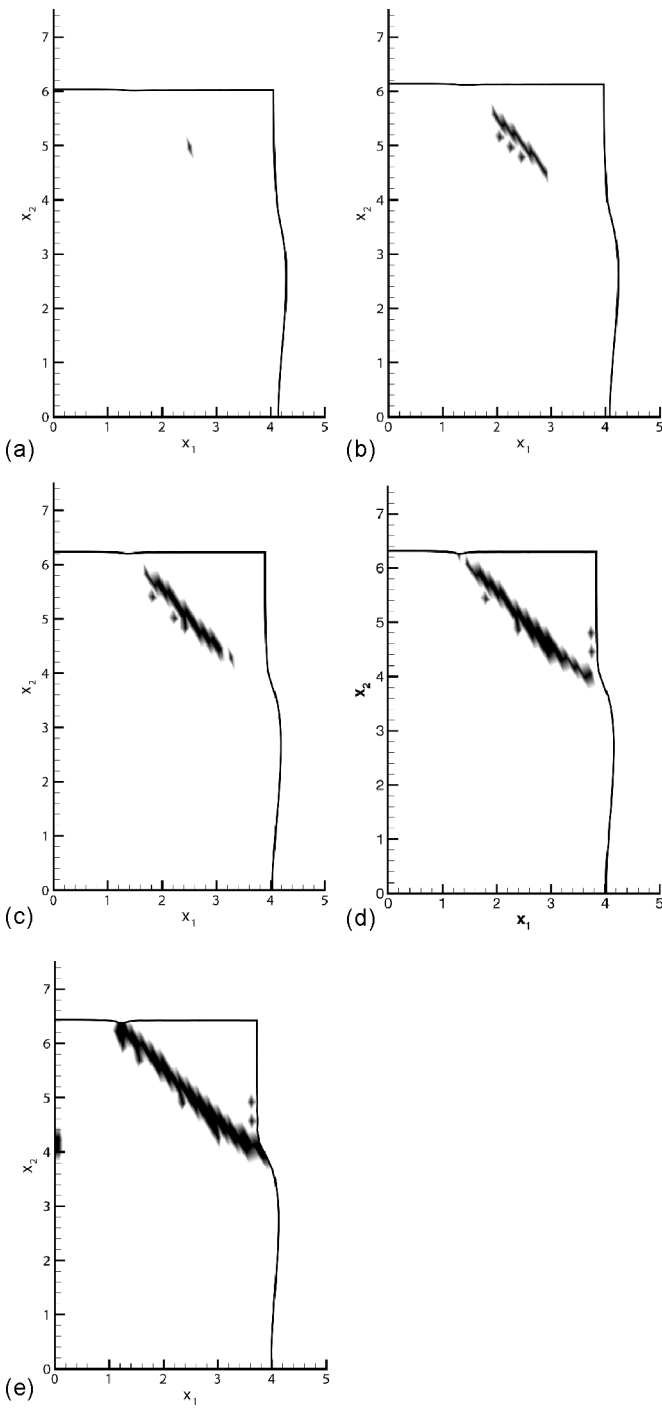


Figure 6. Shear banded region, shown shaded, in a W/NiFe composite with W in the region $r < 5$ and NiFe in $r > 5$ at (a) $42 \mu\text{s}$, (b) $46 \mu\text{s}$, (c) $50 \mu\text{s}$, (d) $54 \mu\text{s}$, and (e) $58 \mu\text{s}$; the effective plastic strain in the red area exceeds 1.0.

1600 uniform elements by less than 2.2%. One could use either adaptively refined meshes (e.g., see [8]) or a meshless method such as the modified smoothed particle hydrodynamics [61] to compute results. The former technique smoothens deformation fields and tends to delay the ASB initiation but gives narrower bands. The latter is computationally less efficient than the FEM.

Other compositional profiles symmetric about the two centroidal axes include $v_{f,NiFe} = a + bX_1^{2p}X_2^{2q}$, where a , b , p , and q are real numbers such that $0 \leq v_{f,NiFe} \leq 1$ for all admissible values of X_1 and X_2 . These have not been examined.

CONCLUSIONS

We have analyzed the initiation and propagation of ASBs in FG bodies deformed in-plane-strain tension at an average axial strain rate of 5000/s. Each FGM studied is composed of two constituents, one of which is tungsten and the other NiFe, copper, 4340 steel, or iron. Several spatial distributions of the two constituents in the region $r \leq H$ are considered. Here r is the radial distance from the centroid of the square cross section of side $2H$. The material is homogeneous in the region $r \geq H$. For uniform 40×40 and 120×120 FE meshes of four-node quadrilateral elements, the ASB initiation time differed by 2.1%. It is found that an ASB initiates either at the specimen centroid or at a point on the top surface where the normal component of velocity is prescribed. In each case, it propagates along the direction of the maximum shear stress. An ASB initiates in an FGM at a lower value of the average axial strain than that in a homogeneous body made of either one of the two constituents. Thus, for the material combinations studied here, the addition to tungsten of a material that is less susceptible to adiabatic shear banding than tungsten enhances the susceptibility of the FGM to adiabatic shear banding. The analysis can thus be used to optimize the compositional profile to either delay or to enhance the onset of an ASB.

REFERENCES

1. H. Tresca, On Further Application of the Flow of Solids, *Proc. Inst. Mech. Eng.*, vol. 30, pp. 301–345, 1878.
2. H. F. Massey, The Flow of Metal During Forging, *Proc. Manchester Assoc. Eng.*, pp. 21–26, 1928.
3. C. Zener and J. H. Hollomon, Effect of Strain Rate upon Plastic Flow of Steel, *J. Appl. Phys.*, vol. 15, pp. 22–32, 1944.
4. R. F. Recht, Catastrophic Thermoplastic Shear, *J. Appl. Mech.*, vol. 31, pp. 189–193, 1964.
5. Y. L. Bai, Thermoplastic Instability in Simple Shear, *J. Mech. Phys. Solid*, vol. 30, pp. 195–207, 1982.
6. R. C. Batra and L. Chen, Effect of Viscoplastic Relations on the Instability Strain, Shear Band Initiation Strain, the Strain Corresponding to the Maximum Shear Band Spacing, and the Band Width in a Thermoviscoplastic Material, *Int. J. Plasticity*, vol. 17, pp. 1465–1489, 2001.
7. A. Marchand and J. Duffy, An Experimental Study of the Formation Process of Adiabatic Shear Bands in a Structural Steel, *J. Mech. Phys. Solid*, vol. 36, pp. 251–283, 1988.
8. R. C. Batra and K. Ko, Analysis of Shear Bands in Dynamic Axisymmetric Compression of a Thermoviscoplastic Cylinder, *Int. J. Eng. Sci.*, vol. 31, pp. 529–547, 1993.
9. R. C. Batra and X. T. Zhang, On the Propagation of a Shear Band in a Steel Tube, *J. Eng. Mater. Tech.*, vol. 116, pp. 155–161, 1994.

10. Y. L. Bai and B. Dodd, *Adiabatic Shear Localization: Occurrence, Theories, and Applications*, Pergamon Press, Oxford, 1992.
11. T. W. Wright, *The Physics and Mathematics of Adiabatic Shear Bands*, Cambridge University Press, Cambridge, 2002.
12. Y. Tomita, Simulation of Plastic Instabilities in Solid Mechanics, *Appl. Mech. Rev.*, vol. 47, pp. 171–205, 1994.
13. R. Armstrong, R. C. Batra, M. Meyers, and T. W. Wright, Shear Instabilities and Viscoplasticity Theories, *Mech. Mater.*, vol. 17, pp. 83–328, 1994.
14. R. C. Batra, Y. D. S. Rajapakse, and A. Rosakis, Failure Mode Transitions under Dynamic Loading, *Int. J. Fract.*, vol. 101, pp. 1–180, 2000.
15. H. M. Zbib, T. Shawki, and R. C. Batra (eds.), *Material Instabilities*, *Appl. Mech. Rev.*, vol. 45, pp. 1–173, 1992.
16. P. Perzyna (ed.), *Localization and Fracture Phenomenon in Inelastic Solids*, Springer-Verlag, Vienna, New York, 1998.
17. R. C. Batra and H. M. Zbib, *Material Instabilities: Theory and Applications*, ASME Press, New York, 1994.
18. D. P. H. Hasselman and G. E. Youngblood, Enhanced Thermal Stress Resistance of Structural Ceramics with Thermal Conductivity Gradient, *J. Am. Ceram. Soc.*, vol. 61, pp. 49–52, 1978.
19. A. Kawaskai and R. Watanabe, Finite Element Analysis of Thermal Stress of the Metals/Ceramics Multi-layer Composites with Controlled Compositional Gradients, *J. Jpn Inst. Metals*, vol. 52, pp. 525–529, 1987.
20. N. Noda and T. Tsuji, Steady Thermal Stresses in a Plate of a Functionally Graded Material, *Proc. 1st Int. Symposium, on Functionally Graded Materials* (Eds M. Yamaouchi, M. Koizumi, T. Hirai, and I. Shiota), Sendai, Japan, pp. 339–344, 1990.
21. Y. Tanigawa, Y. Ootao, and R. Kawamura, Thermal Bending of Laminated Composite Rectangular Plates and Nonhomogeneous Plates due to Partial Heating, *J. Thermal Stresses*, vol. 14, pp. 285–308, 1991.
22. K. Ravichandra, Thermal Residual Stresses in a Functionally Graded System, *Mater. Sci. Eng.*, vol. 201A, pp. 269–276, 1995.
23. N. Noda, Thermal Stress Intensity Factor for a Functionally Graded Plate, *J. Thermal Stresses*, vol. 20, pp. 373–387, 1997.
24. Y. Ootao and Y. Tanigawa, Three-Dimensional Transient Thermal Stresses of Functionally Graded Rectangular Plate due to Partial Heating, *J. Thermal Stresses*, vol. 22, pp. 35–55, 1999.
25. Z. H. Jin and R. C. Batra, Stress Intensity Relaxation at the Tip of an Edge Crack in a Functionally Graded Material Subjected to a Thermal Shock, *J. Thermal Stresses*, vol. 19, pp. 317–339, 1996.
26. Z. Q. Cheng and R. C. Batra, Three-Dimensional Thermoelastic Deformations of a Functionally Graded Elliptic Plate, *Compos. B*, vol. 31, pp. 97–106, 2000.
27. J. N. Reddy and Z. Q. Cheng, Three-Dimensional Thermomechanical Deformations of Functionally Graded Rectangular Plates, *Eur. J. Mech. A—Solids*, vol. 20, pp. 841–855, 2001.
28. S. S. Vel and R. C. Batra, Exact Solutions for Thermoelastic Deformations of Functionally Graded Thick Rectangular Plates, *AIAA J.*, vol. 40, pp. 1421–1433, 2002.
29. S. S. Vel and R. C. Batra, Three-Dimensional Analysis of Transient Thermal Stresses in Functionally Graded Plates, *Int. J. Solid Struct.*, vol. 40, pp. 7181–7196, 2003.
30. Z. G. Zhu and R. C. Batra, Analysis of Shear Banding in Plane Strain Compression of a Bimetallic Thermally Softening Viscoplastic Body Containing an Elliptical Void, *J. Eng. Mater. Tech.*, vol. 113, pp. 382–395, 1991.
31. R. C. Batra and Z. G. Zhu, Dynamic Shear Band Development in a Thermally Softening Bimetallic Body Containing Two Voids, *Acta Mech.*, vol. 86, pp. 31–52, 1991.
32. R. C. Batra and Z. G. Zhu, Dynamic Adiabatic Shear Band Development in a Bimetallic Body Containing a Void, *Int. J. Solid Struct.*, vol. 27, pp. 1829–1854, 1991.
33. R. C. Batra and N. A. Jaber, Failure Mode Transition in an Impact Loaded Prenotched Plate with Four Thermo-viscoplastic Relations, *Int. J. Fracture*, vol. 110, pp. 47–71, 2001.
34. A. L. Gurson, Continuum Theory of Ductile Rupture by Void Nucleation and Growth: Part I, *J. Eng. Mater. Tech.*, vol. 99, pp. 2–15, 1977.

35. Z. P. Wang and Q. Jiang, A Yield Criterion for Porous Ductile Media at High Strain Rate, *J. Appl. Mech.*, vol. 64, pp. 503–509, 1997.
36. Z. P. Wang, Void-Containing Nonlinear Materials Subjected to High-Rate Loading, *J. Appl. Phys.*, vol. 81, pp. 7213–7227, 1997.
37. V. Tvergaard, Influence of Voids on Shear Band Instabilities under Plane Strain Conditions, *Int. J. Fracture*, vol. 17, pp. 389–407, 1981.
38. G. R. Johnson and W. H. Cook, A Constitutive Model and Data for Metals Subjected to Large Strains, High Strain-Rates, and High Temperatures, *Proc. 7th International Symp. on Ballistics*, pp. 541–547, 1983.
39. C. Chu and A. Needleman, Void Nucleation Effects in Biaxially Stretched Sheets, *J. Eng. Mater. Tech.*, vol. 102, pp. 249–256, 1980.
40. V. Tvergaard and A. Needleman, Analysis of the Cup-Cone Fracture in a Round Tensile Bar, *Acta Metall.*, vol. 32, pp. 157–169, 1984.
41. B. Budiansky, Thermal and Thermoelastic Properties of Isotropic Composites, *J. Compos. Mater.*, vol. 4, pp. 701–744, 1990.
42. B. Jiang and R. C. Batra, Effective Properties of a Piezocomposite Containing Shape Memory Alloy and Inert Inclusions, *Cont. Mech. Thermodyn.*, vol. 14, pp. 87–111, 2002.
43. P. Perzyna, Constitutive Modeling of Dissipative Solids for Localization and Fracture, in P. Perzyna, (ed.), *Localization and Fracture Phenomenon in Inelastic Solids*, pp. 99–242, Springer, Berlin, 1998.
44. C. Cattaneo, A Form of Heat Equation Which Eliminates the Paradox of Instantaneous Propagation, *CR Acad. Sci.*, vol. 247, pp. 431–433, 1958.
45. P. Vernotte, The True Heat Equation, *CR Acad. Sci.*, vol. 247, p. 2013, 1958.
46. M. Chester, Second Sound in Solids, *Phys. Rev.*, vol. 131, pp. 2103–2015, 1963.
47. R. C. Batra and M. H. Lear, Adiabatic Shear Banding in Plane Strain Tensile Deformations of Eleven Thermoviscoplastic Materials with Finite Thermal Wave Speed, *Int. J. Plasticity* (in press).
48. R. C. Batra and L. Chen, Instability Analysis and Shear Band Spacing in Gradient-Dependent Thermoviscoplastic Materials with Finite Speeds of Thermal Waves, *Arch. Mech.*, vol. 53, pp. 167–192, 2001.
49. R. C. Batra, On Heat Conduction and Wave Propagation in Non-simple Rigid Solids, *Lett. Appl. Eng. Sci.*, vol. 3, pp. 97–107, 1975.
50. R. C. Batra and K. H. Kim, Effect of Viscoplastic Flow Rules on the Initiation and Growth of Shear Bands at High Strain Rates, *J. Mech. Phys. Solid*, vol. 38, pp. 859–874, 1990.
51. R. C. Batra, Steady State Penetration of Thermoviscoplastic Targets, *Comp. Mech.*, vol. 3, pp. 1–12, 1988.
52. S. R. Bodner and Y. Partom, Constitutive Equations for Elastic-Viscoplastic Strain-Hardening Materials, *J. Appl. Mech.*, vol. 56, pp. 385–389, 1975.
53. T. Mori and K. Tanaka, Average Stress in Matrix and Average Elastic Energy of Materials with Misfitting Inclusions, *Acta Metall.*, vol. 21, pp. 571–574, 1973.
54. P. M. Suquet, Overall Potentials and Extremal Surfaces of Power Law or Ideally Plastic Composites, *J. Mech. Phys. Solid*, vol. 41, pp. 981–1002, 1993.
55. R. C. Batra and D. Rattazzi, Adiabatic Shear Banding in a Thick-Walled Steel Tube, *Comp. Mech.*, vol. 5, pp. 426–442, 1997.
56. R. C. Batra and C. H. Kim, Analysis of Shear Banding in Twelve Materials, *Int. J. Plasticity*, vol. 8, pp. 425–452, 1992.
57. R. C. Batra, Finite Plane Strain Deformations of Rubberlike Materials, *Int. J. Numer. Method. Eng.*, vol. 15, pp. 145–160, 1980.
58. R. C. Batra and X. Q. Liang, Finite Dynamic Deformations of Smart Structures, *Comp. Mech.*, vol. 20, pp. 427–438, 1997.
59. R. C. Batra and Y. W. Kwon, Adiabatic Shear Banding in a Bimetallic Body, *Acta Mech.*, vol. 77, pp. 281–297, 1989.
60. M. Zhou, A. Needleman and R. J. Clifton, Finite-Element Simulation of Shear Localization in Plate Impact, *J. Mech. Phys. Solid*, vol. 42, pp. 423–458, 1994.
61. R. C. Batra and G. M. Zhang, Analysis of Adiabatic Shear Bands in Elastothermoviscoplastic Materials by Modified Smoothed-Particle Hydrodynamics (MSPH) Method, *J. Comp. Phys.*, (in press, available online).